

Constrained $\sqrt{\hat{S}_{min}}$ and reconstructing with semi-invisible production at hadron colliders

Abhaya Kumar Swain and Partha Konar

*Theoretical Physics Group, Physical Research Laboratory (PRL),
Ahmedabad, Gujarat - 380 009, India*
E-mail: abhaya@prl.res.in, konar@prl.res.in

ABSTRACT: Mass variable $\sqrt{\hat{S}_{min}}$ and its variants [1, 2] were constructed by minimising the parton level center of mass energy that is consistent with all inclusive measurements. They were proposed to have the ability to measure mass scale of new physics in a fully model independent way. In this work we relax the criteria by assuming the availability of partial informations of new physics events and thus constraining this mass variable even further. Starting with two different classes of production topology, *i.e.* antler and non-antler, we demonstrate the usefulness of these variables to constrain the unknown masses. This discussion is illustrated with different examples, from the standard model Higgs production and beyond standard model resonance productions leading to semi-invisible production. We also utilise these constrains to reconstruct the semi-invisible events with the momenta of invisible particles and thus improving the measurements to reveal the properties of new physics.

KEYWORDS: [Beyond Standard Model](#), [Standard Model](#), [Hadronic Colliders](#), [Particle and resonance production](#).

Contents

1. Introduction	1
2. $\sqrt{\hat{s}}$ mass-bound variables without additional constraints	4
3. Antler topology and constrained variable	7
4. Non-antler topology and constrained variables	12
5. Event reconstruction capability	13
6. Summary and conclusions	16

1. Introduction

The Standard Model (SM) is now essentially complete after CMS [3] and ATLAS [4] found its last missing bit, lone neutral scalar of the model, the Higgs boson. The SM is so far extremely successful in explaining the fundamental particles and the interactions between them. However some of the unresolved theoretical questions together with very convincing experimental observations, such as dark matter, neutrino oscillation and several others compel us to believe that the SM can not be the complete description. Numerous models beyond Standard Model (BSM) was constructed to accommodate some of these phenomena with a general belief that the scale of new physics is just around the corner at few to multi-TeV level. Unfortunately, large hadron collider (LHC) has not observed any indication of new physics so far. Now, if any of these TeV scale BSM theories exists in nature then it can manifest its signature at the next LHC run. A scenario with positive signal essentially necessitates the determination of the new particle mass, spin and coupling etc associated with that new physics.

Recently popular theoretically appealing BSM theories are the ones which accommodate the thermal relic dark matter as stable and weakly interacting massive particle (WIMP) estimating the tightly constrained observed amount of dark matter density [5]. Hence, this stability of the dark matter in most of the BSM theory is ensured by some discrete symmetry, such as Z_2 symmetry in supersymmetry or many other scenario. Once this symmetry is respected, all the heavy BSM particles in such model has to be produced in pairs; subsequently decaying into some lighter BSM resonance together with SM particles (which may or may not be detected and measured at the detector) in multiple steps of successive decay. Typically at the end of each decay chain lightest BSM particle is produced which is the dark matter particle of that model and escape the detection. Hence, at least two massive and lightest

BSM particles remain hidden in these events. The only way to know their presence is the observation of sizable \vec{P}_T in the detector calculated from the imbalance of transverse visible momenta produced in such events. The reconstruction of a dark matter signal at hadronic collider is challenging because of the partial knowledge of the incoming parton momenta further burdened with multiple massive final state particles of unknown mass goes undetected keeping no individual momentum informations at the detector.

There has been several studies under gone into mass and spin determination in the context of semi-invisible production at the hadronic collider¹ and we classify them based on the topology information as follows:

Exclusive variables are defined based on the topology of the production mechanism and decay processes under consideration. Identical signatures consists of visibles and invisibles in the final state can be originated from very different topologies which is deeply related to the stabilising symmetry of the dark matter (DM). Shape of the visible invariant mass can effectively carry informations on topology along with the mass spectrum [9] of the decay chain. Underlying DM stabilising symmetry can also be probed [10–12] using kinematic edge and cusp in the invariant mass distributions and from the shapes of transverse mass variable M_{T2} . Even the assumption of one particular underlying symmetry allows some fixed number of different topologies from which the correct one can be identified comparing suitable kinematic variables [13]. One expects that the ignorance of the correct topology can add difficulties in solving combinatorial ambiguity [14–17] which is one source of complexity in mass determination methods, more prominently available when associated with long decay chain. This ambiguity can be originated from two different sources. Firstly, allocation of the final state particles to the correct decay chain, *i.e.* from which side of the decay chain some particular states is produced. Secondly, the ordering of the assigned particle in a single decay chain. The hemisphere method [18] and PT vs M methods [15] are introduced to reduce the this ambiguity in assigning the correct final state particles to the corresponding decay chain. However, the ordering of the particles left unresolved. The M_{T2} variable together with invariant mass are also shown to reduce the combinatorics significantly [16]. In the literature several classes of exclusive variables are defined assuming that the correct knowledge of topology is available and anticipating that the combinatorial ambiguity can be controlled. The exclusive mass determination methods can be categorised as follows

- *Edge measurement method:* Based on the idea of constructing all possible invariant masses out of visible decay products in each decay chain [19–25]. Each invariant mass has an endpoint which is experimentally observable and these endpoints are related to the unknown masses in the decay chain. To evaluate all the unknown masses by inverting the the equations in terms of measured endpoints, one needs sufficient number of independent endpoint measurements. So essentially a long decay chain is necessary to have unique measurement of all the unknown masses. However this criteria inevitably invites combinatorial ambiguity thereby reducing the effectiveness of the method. This

¹For some recent review, see ref. [6–8]

method also does not use all the available informations like missing transverse momentum \vec{P}_T in the event.

- *Polynomial method*: One tries to utilise all the available information in the event of particular topology and solve for the unknown masses and momentums [26–30] considering on-shell cascade decay. In the literature, typically the production of two heavy invisible particle is considered at the final state, assuming Z_2 type of DM stabilising symmetry in the theory. All the unknown invisible momenta components are solved utilising mass-shell constraints and missing \vec{P}_T constraints in the event. It can be shown that one needs to consider long decay chains to solve for all unknowns in the event. Combinatorial ambiguity naturally arises here from the requirement of the long decay chain. Moreover, resulting invisible momenta remain ambiguous due to existence of multiple solutions originating from non-linear mass-shell constraints [30, 31].
- *Transverse mass variable*: Rather than considering full event information, transverse projection of momenta is considered during calculation. Contrary to previous cases, even small decay chain can constrain the masses realistically. There are many variants of transverse mass variable exist in the literature such as M_{T2} [32–40], M_{T2}^{sub} [41], M_{CT2} [42, 43], 1D orthogonal decomposition of M_{T2} ($M_{T2\perp}$ and $M_{T2\parallel}$) [44], asymmetric M_{T2} [45, 46] and M_{T2}^{approx} [47], M_{CT} [48–50], and variants $M_{CT\perp}$ and $M_{CT\parallel}$ [51] etc. Among these broad class of transverse mass-bound variables, we briefly discuss some properties of M_{T2} which is studied widely in the literature. This variable is defined as the constrained minimisation of maximum of two transverse masses M_T from both sides of the decay chain. The minimisation is done over all possible partitions of missing transverse momenta where as, satisfying the \vec{P}_T constraint. $M_{T2}(\tilde{m}_{inv})$ expressed as a function of the unknown invisible particle mass, can have an experimentally observed upper bound over many events. This provides a useful correlation between the trial invisible mass \tilde{m}_{inv} and measured upper bound M_{T2}^{max} , which represents the corresponding mass of the ancestor particle (commonly called as mother or parent) responsible for producing all the visible and the invisible particles within the (sub)system. This correlation also satisfy the true yet unknown mass parameters fulfilling the crucial equality $M_{T2}^{max}(m_{inv}^{true}) = m_{mother}^{true}$. Interestingly, one can measure the true mass of both mother and daughter simultaneously by identifying a discontinuity (kink) arises due to additional conditions like two step decay chain [36, 37], extra upfront P_T from ISR [38, 39] or in subsystem context [41]. Extracting these kinematic endpoint is occasionally troublesome with thinly populated events at the endpoint, and in presence of backgrounds. Available on-shell constraints of intermediate particles can be exploited in the (1+3) dimensional variable M_2 [52, 53] to improve number the events appearing at the tail of these distributions.

Global and inclusive variable are independent of topology information and hence, do not require any information about the production mechanism of the particles in the event. Variables are constructed using only visible particles momenta and missing transverse momenta

in the event. Several of them were well known and utilised for long as event selection variables *e.g.* H_T [54], total visible invariant mass M [55], effective mass M_{eff} , total transverse component of invisible momentum \cancel{E}_T , total visible energy E and total transverse energy E_T in the event. Lately introduced \hat{s}_{min} [1] and its variants \hat{s}_{min}^{sub} and \hat{s}_{min}^{reco} [2] are also constructed as global and inclusive variable for measuring mass scale of new physics. Being a topology independent variable, they are also applicable to any possible decay chain without worrying about the symmetric and asymmetric topology and simple analytical form is also available. Thus any generic topology can be assimilated without affected by the combinatorial ambiguity. We would discuss further about these variables in Sec. 2.

In this present work our objective is to demonstrate the usefulness of partial event informations including the topology in the variables like \hat{s}_{min} which were constructed as global one. After an introduction of analytic form for these variables in Sec. 2, we discuss effects of additional constrains for two topology classes based on the production and decay of heavy resonance. Antler topology being one important topology for single resonant production, have considerable discovery potential in different SM and BSM modes. This class can be constrained significantly and some interesting features can be noticed. In Sec. 3 we motivate and discuss the constraints. We would notice the constrained variable \hat{s}_{min}^{cons} can notably improve the distribution. Second interesting takeaway from these constraints is that not only the minimum quantity \hat{s}_{min} , but one can also construct a maximum quantity \hat{s}_{max} which is also bounded. Hence, one additional variable \hat{s}_{max}^{cons} can be defined and finite since these constraints play a critical role. After construction of these constrained variables we display how they were restricted in several events. In the next section, Sec. 4 we consider similar variables in case of non-antler topology. In Sec. 5 we turn to the capability of these variable in reconstructing the events. M_{T2} assisted method (known as MAOS) [56, 57] is proposed earlier by utilising the transverse components of the invisible momenta obtaining from the minimisation of this transverse mass. Whereas, longitudinal components are solved using the on-shell constraints and thus having two fold ambiguity from each decay chain. Recently proposed some of the (1+3) dimensional M_2 [53] variables can lead to unique momentum reconstruction for symmetric topology where additional constraints over equality of mother and on-shell relative take a pivotal role. Here in the reconstruction from the minimisation of \hat{s} does not rely on any particular topology and can be used for any of the symmetric or asymmetric cases for a unique solution. We would further demonstrate that the inclusion of additional constraints also improve these reconstructed momenta. We summarize and conclude at the end.

2. $\sqrt{\hat{s}}$ mass-bound variables without additional constraints

Let us start by discussing briefly about the variable $\sqrt{\hat{s}_{min}}$ which was first introduced [1] to determine the mass scale associated with any generic process (or event topology) involving missing particles. It is inspired from the fact that the precise knowledge of partonic system center of mass (CM) energy $\sqrt{\hat{s}}$ carries the kinematic informations like masses of heavy resonance, or threshold of pair productions at the hadron collider. Hence, one may like to know

the distribution of this variable even approximately, after recognising the fact that there is no way we can completely reconstruct the event, or extract all the momentum informations in case of general semi-invisible productions at the hadron collider. Utilising all the experimentally observed quantities, best one gets the minimum partonic CM energy which is compatible (or consistent) with the observed visible momenta and missing transverse momentum. Although general event topology can have a wide diversity in production mechanism of visibles and invisibles and also number of them, it emerged that the final minimisation leads to a rather simple and versatile functional form for $\sqrt{\hat{s}_{\min}}$.

This variable was further extended [2] to apply in general subsystems, and also utilised reconstructed events to safe guard the generic variables from underlying events and ISR [58, 59]. Subsequently these $\sqrt{\hat{s}}$ variables were shown and classified [7, 60] as M_1 type of mass-bound variables represented in a compact nomenclature of M_{\dots} class of variables. Wide variety within this class are constructed systematically considering different projection methods, additional second projection [44, 51], and considering different orders of the operations. Interestingly, most of the existing mass variables devised based on different utility can be accommodated in this unified picture, leaving many more new variable elements in this class hitherto unexplored.

One can simplify the discussion under the following assumptions which are rather common in wide class of BSM models: (i) The DM stabilisation is respected by discrete Z_2 symmetry. As a result, all BSM particles in the theory would produce in pair leading to two stable DM particles in the final state. They stay invisible in the detector resulting missing transverse energy as their combined footprint. (ii) There is only one DM candidate in the theory, or if multiple DM particles are there then they are degenerate in mass. One can note that even after making these two assumption the variable \hat{s}_{\min} remains global and inclusive.

Under these assumptions analytic expression and properties of this mass-bound variable $\sqrt{\hat{s}_{\min}}$ can be discussed using the non-antler topology displayed² in Fig. 1. In the (sub)system under consideration, two mothers denoted by the B_1 and B_2 either produced in hard scattering at the hadron collider, or starting point in the subsystem from a event with longer decay chain. Eventually each of these mothers decays to produce two visible and one invisible particle. The topology can also contain intermediate particles which may be on-shell or off-shell, symbolising into the blue bulb to show the final products only. Momenta p_j of these visible SM particles V_j ($j = 1, \dots, 4$) represented by blue lines can be measured at the detector. On the contrary, the invisible particles X_i ($i = 1, 2$) in black dashed lines are of BSM nature with individual mass m_i , and 3-momenta q_i . The partonic Mandelstam variable for this topology is given by,

$$\hat{s} = \left(E^v + \sum_{i=1}^{n_{inv}} \sqrt{m_i^2 + \vec{q}_{iT}^2 + q_{iz}^2} \right)^2 - \left(P_z^v + \sum_{i=1}^{n_{inv}} q_{iz} \right)^2 \quad (2.1)$$

²In general, there can be any number of visibles including asymmetric production topology or asymmetric invisibles (*e.g.* as in [46]) in the final state, but here we restrict our discussion for simplicity and as a reference for proceeding discussion in following sections. We refer ref. [1, 2] for a most generic representation for which these $\sqrt{\hat{s}}$ variables are constructed and applicable.

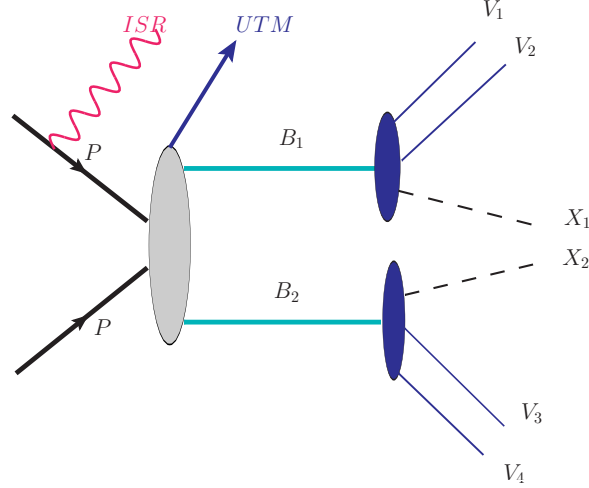


Figure 1: Representative for a simple non-antler topology where after production of two heavy mother particles B_α , each of them leading to single invisible massive particle X_i together with number of visibles V_j in the final state. The blue bulb represents the intermediate particle which may be off-shell or on-shell. The visible particles are SM particles measurable at the detector and represented by blue lines denoted by V_1, V_2, V_3 and V_4 respectively. The invisible particles are represented by black dashed lines denoted by X_1 and X_2 respectively. The momenta of visibles and invisibles are denoted by $p_i, i = 1, 2, 3, 4$ and $q_j, j = 1, 2$.

Here, $n_{inv} = 2$ is the number of invisible particles, $E^v = \sum_j e_j^v$ and $P_z^v = \sum_j p_j^z$ are total energy and total longitudinal component of the visible momenta. In the above equation missing transverse momentum constraints $\vec{P}_T = \sum_i \vec{q}_{iT}$ are also taken into account. Clearly even in this simplified case, there are $3n_{inv} = 6$ unknown momenta components, as well as unknown invisible mass with only two constraints from missing transverse momentum. So one can not hope to calculate true values of \hat{s} involved event by event. But it is important to realise that there is an absolute minimum exist for \hat{s} in each event which also satisfy all these observable. By minimizing \hat{s} with respect to unknown momenta \vec{q}_i subject to the missing \vec{P}_T constraints one gets

$$q_{iT} = f_m^{(i)} \vec{P}_T, \quad (2.2)$$

$$q_{iz} = f_m^{(i)} \frac{P_z^v}{\sqrt{(E^v)^2 - (P_z^v)^2}} \sqrt{M_{inv}^2 + \vec{P}_T^2}. \quad (2.3)$$

$f_m^{(i)}$ is a dimensionless mass fraction varies between 0 and 1 and is given by $f_m^{(i)} = \frac{m_i}{M_{inv}}$ and total sum of all invisible masses $M_{inv} = \sum_{i=1}^{n_{inv}} m_i$. Now replacing the above expression of q_{iT} and q_{iz} in \hat{s} one gets the final form of \hat{s}_{min} as

$$\sqrt{\hat{s}_{min}(M_{inv})} = \sqrt{(E^v)^2 - (P_z^v)^2} + \sqrt{\vec{P}_T^2 + M_{inv}^2}. \quad (2.4)$$

One can follow from the computation that the \hat{s}_{min} does not assume any particular event topology or the DM stabilising symmetry of the model. Based on common BSM scenario,

we restrict our description (also in Fig. 1) assuming Z_2 symmetry, so that, pair production of BSM particles are considered producing two invisible massive particles in the final states. From minimisation conditions in Eq. 2.2 and 2.3 one can infer that each DM particle carries a fraction of missing momenta, proportional to the corresponding mass fraction $f_m^{(i)}$. However final \hat{s}_{\min} is simply a function of total M_{inv} irrespective to this fraction. Once we assume a pair of invisibles in the final state with same mass (or both massless), then this fraction $f_m^{(i)}$ comes out as $1/2$ for any choice of trial mass³ including the true invisible mass. The invisible momenta at the minimisation are,

$$q_{iT} = \frac{1}{2} \vec{P}_T, \quad (2.5)$$

$$q_{iz} = \frac{1}{2} \frac{P_z^v}{\sqrt{(E^v)^2 - (P_z^v)^2}} \sqrt{M_{inv}^2 + \vec{P}_T^2}. \quad (2.6)$$

These invisible momenta calculated from minimisation may not represent that of the true event. However the uniqueness of these momenta can be useful to study the semi-invisible decays involved both in SM as well as BSM scenario. Momentum reconstruction can be exploited to analyse the properties of top quark decaying invisibly in the SM, whereas DM motivated BSM models are commonplace where uniqueness of invisible momenta can help to study decays with different topology. One can notice that the invisible momenta constructed through \hat{s}_{\min} are always parallel to each other with a magnitude proportional to mass fraction. Here we investigate how the partial knowledge of event information can improve the variable \hat{s}_{min} and also reconstructed momentum obtained from it. In our further discussion, we divide the production topology as two kinds, such as, antler topology and non-antler topology. We discuss \hat{s}_{min} with and without putting on-shell constraints in both kinds of these topology.

3. Antler topology and constrained variable

Antler topology is very common and well motivated in SM Higgs production. Resonant Higgs production and its semi-invisible decays into W-boson, $h \rightarrow WW^* \rightarrow l\nu l\nu$ or through τ decay $h \rightarrow \tau\tau \rightarrow w\nu_\tau w\nu_\tau$ are some of the interesting channels. Several popular BSM scenario also have these production, such as, supersymmetric (SUSY) heavy Higgs decays through neutralinos $H \rightarrow \tilde{\chi}_2^0 \tilde{\chi}_2^0 \rightarrow Z \tilde{\chi}_1^0 Z \tilde{\chi}_1^0$ [61], or SUSY Z' production with leptonic decay $Z' \rightarrow \tilde{\ell}^+ \tilde{\ell}^- \rightarrow \ell^- \tilde{\chi}_1^0 \ell^+ \tilde{\chi}_1^0$ [62, 63]. In the model of universal extra dimension (UED) one can produce resonant second excitation states decaying into couple of lighter states, like $Z^{(2)} \rightarrow L^{(1)} L^{(1)} \rightarrow \ell^- \gamma^{(1)} \ell^+ \gamma^{(1)}$ [64, 65]. Other class of examples being resonant exotics production with their semi-invisible SM decay. Doubly charged scalar in hadron collider can decay with one of the dominant decay channel into w -pair, $\phi^{++} \rightarrow w^+ w^+ \rightarrow \ell^+ \nu_\ell \ell^+ \nu_\ell$ [66]. Similarly heavy Higgs or heavy Z' can have SM semi-invisible decay $H/Z' \rightarrow t\bar{t} \rightarrow b\bar{b} w^+ w^- \rightarrow$

³Although, the mass fraction $f_m^{(i)}$ appear to be singular for a choice of zero invisible masses, but one can recalculate starting with a massless scenario and minimizing to get the fraction $f_m^{(i)} = \frac{1}{2}$. Alternatively, from this present expression with arbitrary masses, one can first use the equality of unknown invisible masses before setting it to zero to get back the same fraction.

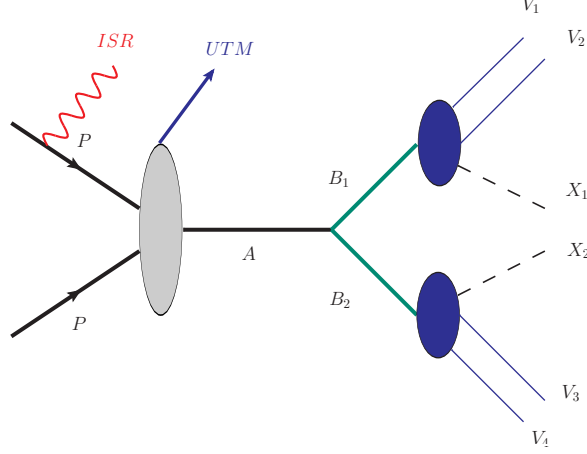


Figure 2: Representative for a simple antler topology where A is a Z_2 parity even heavy resonance produces and decays to two daughter particles B_1 and B_2 and each of which finally decays to two SM visibles V_j and one invisible particle X_i .

$b\bar{b}\ell^+\nu_\ell\ell^-\bar{\nu}_\ell$. Some of these antler topology was studied [67–69] showing that the invariant mass, transverse momenta and angular correlations constructed out of visible decay products are effective to measure the invisible and intermediate particle masses whereas heavy resonant mass is assumed to be known. Cusp and kink structures appeared in the distributions of these variables and their positions are also related to the unknown masses. Missing transverse momentum constraints are not used in these study. Production mechanism in a linear collider (e^+e^-) with a fixed center of mass energy is also very similar to this antler decay topology and semi-invisible decays can be studied in similar fashion [70].

Representative diagram for antler topology is shown in Fig. 2. Parity even heavy resonant state A , produced through on-shell production at the hadron collider, promptly decays to pair of parity odd particles B_1 and B_2 . In this simplified picture, each B subsequently decays same way as we have described earlier in Fig. 1, and thus producing couple of visible with an indivisible daughter. We also keep the same notation for momentum assignment associated to all final particles. Before defining the \hat{s}_{min} in presence of the additional constraints, we first list all the constraints available for this present topology. Apart from the antler resonance mass-shell constraint at some fixed value of the \hat{s} depending upon resonant mass M_A ,

$$(\sum_j p_j + \sum_i q_i)^2 = M_A^2 = \hat{s}^{True}, \quad (3.1)$$

additional mass equations and missing transverse momentum relations for this topology can be put together as, $\{constraints\}$:

$$(p_1 + p_2 + q_1)^2 = M_{B_1}^2, \quad (p_3 + p_4 + q_2)^2 = M_{B_2}^2, \quad (3.2)$$

$$q_1^2 = M_{X_1}^2, \quad q_2^2 = M_{X_2}^2, \quad (3.3)$$

$$\vec{q}_{1T} + \vec{q}_{2T} = \vec{P}_T. \quad (3.4)$$

$\{M_{B_1}, M_{B_2}\}$ and $\{M_{X_1}, M_{X_2}\}$ are the masses⁴ of the intermediate particles $\{B_1, B_2\}$ and the invisible particles $\{X_1, X_2\}$ respectively. Clearly, using the above constraints in Eqs. 3.2-3.4 one can reduce the number of free parameter at two. Afterword in Sec. 5, we would further demonstrate the constrained regions in these parameter space. One can also notice that in the Eqs. 3.2 the ordering of the particle in a particular decay chain does not affect the constraints but assigning particle to decay chain does. The combinatorial ambiguity of later type is severe when one has long decay chain which is absent in our analysis. In general, this type of problem can be partially controlled using existing methods like hemisphere method [18] and PT vs M methods [15].

Now we are in a position to formulate a new variable dubbed as \hat{s}_{min}^{cons} defined as the minimum partonic Mandelstam variable which satisfies all above *constraints* in the event.

$$\hat{s}_{min}^{cons} = \min_{\substack{\vec{q}_1, \vec{q}_2 \\ \{constraints\}}} [\hat{s}(\vec{q}_1, \vec{q}_2)] \quad (3.5)$$

Among all constraints defined in the Eqs. 3.2-3.4, the variable \hat{s}_{min} is already satisfies last four constraints comprising two missing \vec{p}_T components and two mass-shell constraints from invisible daughters. In other words, new variables are further constrained with mass-shell relations of intermediate parents.

The true value of partonic Mandelstam variable for antler topology is the mass of the heavy resonance, that is $\sqrt{\hat{s}^{True}} = M_A$, once the heavy resonance produced on-shell and having narrow decay width. Hence, any mass bound variable constructed by minimisation, such as, \hat{s}_{min} for antler topology needs to be bounded from above satisfying the relation $\hat{s}_{min} \leq \hat{s}^{True}$. This end point can be measured from the endpoint at the distribution over many events. Constrained variable \hat{s}_{min}^{cons} also satisfy similar relation $\hat{s}_{min}^{cons} \leq \hat{s}^{True}$, having endpoint at the \hat{s}^{True} . However additional intermediate particle mass-shell constraints ensure a larger value of \hat{s}_{min}^{cons} over \hat{s}_{min} for each event. This inequality would also reflect in the mass variable distributions contributing larger number of events at the endpoint of the distribution.

As we discussed earlier, a rather striking consequence of this additional mass-shell constraints are that they also permit us to construct a finite upper mass bound variable, which is meaningless otherwise. We define this constrained variable \hat{s}_{max}^{cons} as the maximum partonic Mandelstam variable,

$$\hat{s}_{max}^{cons} = \max_{\substack{\vec{q}_1, \vec{q}_2 \\ \{constraints\}}} [\hat{s}(\vec{q}_1, \vec{q}_2)] \quad (3.6)$$

satisfying all the available *constraints* in the event listed in Eqs. 3.2-3.4, which, in turn, is the maximum of the physically allowed region. Since \hat{s}^{True} satisfies all the available constraints

⁴Note that through out the analysis we have assumed both the intermediate and daughter masses are known and used their true masses in the *constraints*. However, in a scenario when the invisible particle mass is unknown, one can go ahead with the constrained variables assuming some trial mass ($\bar{M}_{X_1}, \bar{M}_{X_2}$) in Eqs. 3.3. One can then expect a correlation between this trial invisible mass with the endpoints in constrained variable distributions.

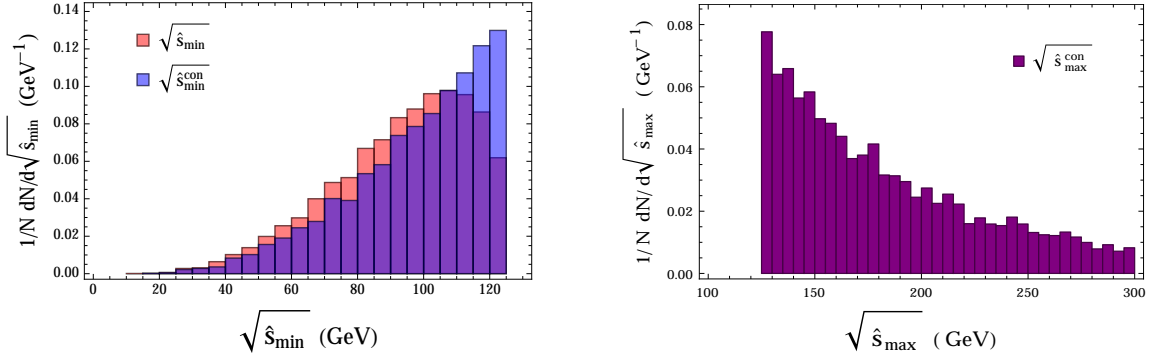


Figure 3: (Left) Figure shows the distribution of \hat{s}_{min} and \hat{s}_{min}^{cons} with $\hat{s}^{True} = M_h = 125.0$ GeV. The red colored histogram is for analytical formula of \hat{s}_{min} which also can be verified using numerical minimisation, blue colored histogram is \hat{s}_{min}^{cons} calculated using numerical minimisation. The variables \hat{s}_{min} and \hat{s}_{min}^{cons} have endpoint at the heavy resonance mass M_h but \hat{s}_{min}^{cons} have larger number of events because of extra constraints it uses in its minimisation. (Right) Figure shows the distribution of the \hat{s}_{max}^{cons} , as one can see it has threshold at the true mass of the heavy resonance $M_h = 125.0$ GeV. As one can see the \hat{s}_{max}^{cons} always greater than or equal to \hat{s}^{True} . Similar unconstrained variable *i.e.* \hat{s}_{max} is not present.

in the event, it must remain within this region. Now, by definition, \hat{s}_{max}^{cons} is where \hat{s} is maximum inside this region and \hat{s}_{min}^{cons} is where it is minimum. So, \hat{s}^{True} can maximally reach up to \hat{s}_{max}^{cons} . Hence, \hat{s}_{max}^{cons} has a lower bound at the \hat{s}^{True} , significantly with a large number of events at this threshold. Interesting point about these constrained \hat{s} variables are that the reconstructed momenta from their minimisation(maximisation) not only unique but they also improve over the same calculated through \hat{s}_{min} . In case of \hat{s}_{min}^{cons} , better momentum reconstruction ensured by the points closer to its endpoint. Similarly, \hat{s}_{max}^{cons} gives better reconstruction from the points associated to its threshold. These points would be discussed further in the Sec. 5, where these correlations would be more evident. Finally, the definitions of different \hat{s} variables, after imposing different constrains, ensures the hierarchy among these mass variables:

$$\hat{s}_{min} \leq \hat{s}_{min}^{cons} \leq \hat{s}^{True} \leq \hat{s}_{max}^{cons}. \quad (3.7)$$

To illustrate the properties of these constraint variables, first we consider a simple example of SM Higgs production through gluon fusion at the hadron collider. Higgs boson decays further semi-invisibly through tau pair production, $h \rightarrow \tau\tau \rightarrow w\nu_\tau w\nu_\tau$. To compare with the representative diagram for the antler production in Fig. 2, τ being the intermediate particle B_i , for which additional mass-shell condition used in the minimisation(maximisation) of constrained \hat{s} . Neutrino ν_τ is the invisible particle X_i . We considered hadronic (leptonic) decay mode for the W boson thereafter to consider two invisibles (four invisibles tested in next example) in the final state. The distribution of \hat{s}_{min} and \hat{s}_{min}^{cons} are shown in the Fig. 3(left). Red binned histogram shows the distribution for \hat{s}_{min} , which can be calculated numerically or using analytical expression. Blue histogram shows the distribution of constrained \hat{s}_{min}^{cons} . As expected the the endpoint of both the \hat{s}_{min} and \hat{s}_{min}^{cons} distributions are at the $\sqrt{\hat{s}^{True}} = M_h = 125$ GeV for a choice of invisible mass as zero. Evidently larger number of events at the endpoint for the \hat{s}_{min}^{cons} distribution with a sharper drop can be measured

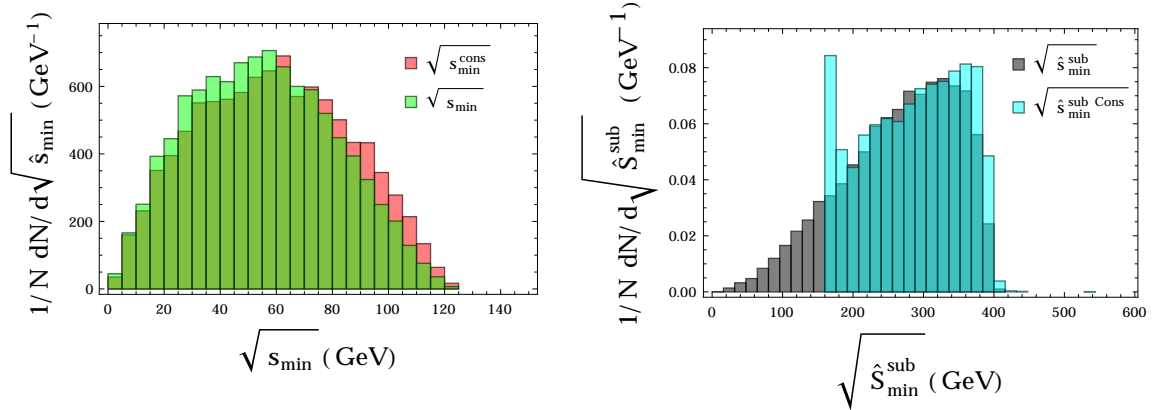


Figure 4: (Left) In this figure we have shown the distribution of the \hat{s}_{\min} and $\hat{s}_{\min}^{\text{cons}}$ for four invisible particle in the final state. The red colored histogram shows the distribution of $\hat{s}_{\min}^{\text{cons}}$ and the green colored histogram shows the distribution \hat{s}_{\min} . As one can see though there are endpoint feature for both the variables but the number events is very less and the improvement for $\hat{s}_{\min}^{\text{cons}}$ over \hat{s}_{\min} is also very less. (Right) Here the red colored histogram is $\hat{s}_{\min}^{\text{sub}}$ calculated using analytical formula, the blue colored histogram is $\hat{s}_{\min}^{\text{sub}}$ calculated numerically and the green colored histogram is $\hat{s}_{\min}^{\text{sub, cons}}$ calculated numerically. The variable $\hat{s}_{\min}^{\text{sub}}$ and $\hat{s}_{\min}^{\text{sub, cons}}$ has endpoint at $\hat{s}_{\min}^{\text{sub, True}} = M_{\phi^{++}}$.

more precisely. This is even more important once corresponding background also considered together. The Fig. 3(right) demonstrates the distribution of other constraint variable $\hat{s}_{\max}^{\text{cons}}$ which has a threshold at \hat{s}^{True} with considerable number of events at the threshold.

It is expected that the endpoint of kinematic distribution would be less populated if one has more number of invisibles in the event. This is because increasing number of invisibles would increase the number of unknown momentums restricted with the same constraints. Following our previous example, we now consider the four invisible particle by decaying both w leptonically and demonstrated corresponding \hat{s}_{\min} and $\hat{s}_{\min}^{\text{cons}}$ distributions in Fig. 4(left). The red histogram shows the distribution for $\hat{s}_{\min}^{\text{cons}}$, whereas the green binned histogram shows \hat{s}_{\min} to compare the effect due to the extra constraints. These distribution confirms that the number of events at the endpoint are considerably low as one increases the number of invisible particle in the final state. Although constrained variable can improve the situation only slightly, overall both these distributions forms a narrow tail rather than the sharp endpoint.

We further study one more interesting example from the resonant production of exotic doubly charged scalar [66] production at the hadron collider following its decay into dominant decay channel producing pair of w , which in turn decays leptonically. Hence, the resonant sub-system under consideration is $\phi^{++} \rightarrow w^+ w^+ \rightarrow \ell^+ \nu_\ell \ell^+ \nu_\ell$. In hadron collider this exotic state ϕ^{++} can be produced associated with charged w^- which mainly decays hadronically and it is possible to disentangle from the antler sub-system producing lepton pair from the exotic decay. We choose to use corresponding subsystem variable $\hat{s}_{\min}^{\text{sub}}$ for our analysis. Here

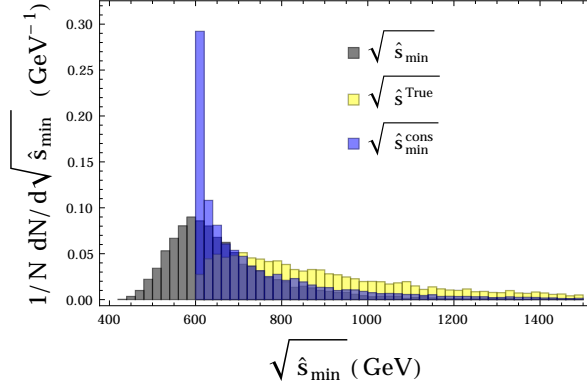


Figure 5: Figure shows the distribution of \hat{s}_{min} (black) and \hat{s}_{min}^{cons} (blue) considering a toy model of non-antler pair production at the the hadron collider, with parent and invisible mass as 300 GeV and 200 GeV respectively. Non-antler heavy parent particle pair production must have a true parton level CM energy distribution starting from a threshold value of total parents mass as shown by yellow colored histogram. As a consequence of additional constraints \hat{s}_{min}^{cons} distribution also poses this same threshold, however with a considerable number of events at the threshold.

analytical expressions for the invisible particle momenta remain same except the modified form for \vec{P}_T which includes the visible contribution from non-sub-system [2]. The distributions for the \hat{s}_{min}^{sub} and the constrained variable $\hat{s}_{min}^{sub,cons}$ are demonstrated in the Fig. 4(right). Dark binned histogram represents the distribution for \hat{s}_{min}^{sub} which can be calculated both analytically or using numerical minimisation. The cyan colored histogram is the distribution for $\hat{s}_{min}^{sub,cons}$ utilising extra w mass-shell constrains, and minimised numerically. One can note that the $\hat{s}_{min}^{sub,cons}$ is performing better in getting the endpoint at ϕ^{++} mass. Observed small tail is because of finite width from ϕ^{++} and these extra constraints ensures that the $\hat{s}_{min}^{sub,cons}$ distribution starts from a threshold at the scale of $2m_w$.

4. Non-antler topology and constrained variables

Non-antler topology is extremely common in most of the BSM theories and also abundant in SM. This topology is already described in the Fig. 1, where B_i are the parent particles produced in pair. After a cascade of decay each side of the decay chain produces number of visibles along with a massive invisible particle X_i . Detailed discussion on the behaviour of \hat{s}_{min} as a mass bound variable is done extensively for this kind of topology. Here we would illustrate the constrained variables in the light of additional on-shell constraints. Unlike using these exact on-shell constraints for the parents mass, which is primarily one would like to know through these mass bound variables, ref. [53] uses constraints from the equality of two parents mass. Following our analysis in previous section, we continue using these mass-shell constraints with an expectation of improved momentum reconstruction.

As a consequence of on-shell constraints, one can expect \hat{s}_{min}^{cons} distribution would start from a threshold at the sum of parents mass. This is contrary to the unconstrained \hat{s}_{min} distribution which exhibits peak at that position giving an excellent correlation for the new physics mass scale. This is demonstrated in Fig. 5 where distributions for \hat{s}_{min} (black) and \hat{s}_{min}^{cons} (blue) are plotted using a toy model of non-antler pair production at the hadron collider, with parent and invisible mass as 300 GeV and 200 GeV respectively. Unlike antler decay topology where heavy particle resonant production form a near delta function at the parton level center of mass energy, here heavy parent particle pair production has a distribution starting from a threshold value of total parents mass as shown by yellow colored histogram. As we note that the \hat{s}_{min}^{cons} distribution also poses this same threshold, however with a considerable number of events at the threshold. We will follow further in the next section to show the improvements in invisible momentum construction as a presence of these constraints and the events contributing at the threshold. Analogous to the variables constructed for antler topology, one can follow the similar hierarchy among all the constrained \hat{s} mass variables after imposing different constrains:

$$\hat{s}_{min} \leq \hat{s}_{min}^{cons} \leq \hat{s}^{True} \leq \hat{s}_{max}^{cons}. \quad (4.1)$$

5. Event reconstruction capability

In this section we describe the invisible momentum reconstruction capability using mass variables \hat{s}_{min} and improvement in it accounting for additional constraints in the context of antler and non-antler decay topology. Analytic expressions for invisible momenta components from the \hat{s}_{min} was already discussed in Sec. 2. It was also argued that these reconstructed invisible momenta using \hat{s}_{min} are unique irrespective of any topology considered. Note that these reconstructed momenta from the minimisation of \hat{s}_{min} are not the true momenta, but approximated momenta consistent with the observables in such event. These calculated momenta can be correlated with the true values of them to find the reconstruction efficiency similar to the other reconstruction methods like MAOS [56, 57].

To describe the consequence of the constraints given in Eqs. 3.2-3.3 in constructing the new variables \hat{s}_{min}^{cons} and \hat{s}_{max}^{cons} , we reorient them to write unknown longitudinal momenta in terms of their transverse components \vec{q}_{iT} . We get,

$$q_{iz} = \frac{\Sigma_i P_{iz}^V \pm E_i^V \sqrt{\Sigma_i^2 - (E_{iT}^V E_{iT}^q)^2}}{(E_{iT}^V)^2}, \quad (5.1)$$

with

$$\Sigma_i = \frac{M_{Bi}^2 - M_{Xi}^2 - M_{vi}^2}{2} + \vec{P}_{iT}^V \cdot \vec{q}_{iT}, \quad (5.2)$$

$$E_{iT}^V = \sqrt{M_{vi}^2 + (p_{iT}^V)^2}, \quad (5.3)$$

$$E_{iT}^q = \sqrt{M_{Xi}^2 + q_{iT}^2} \quad (5.4)$$

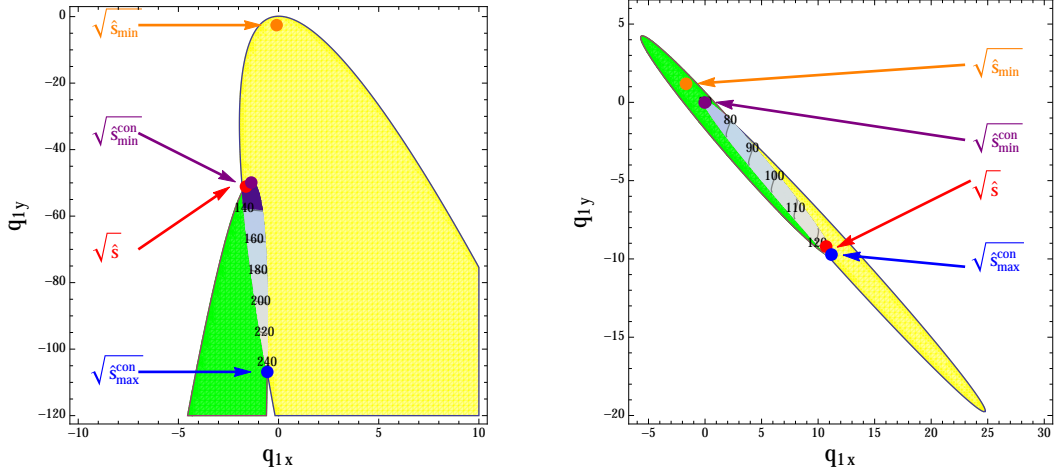


Figure 6: Some example events demonstrating the invisible momentum reconstruction in case of antler topology through minimisation during construction of different \hat{s} variables. Each color shaded region is representing the allowed phase space by additional constrains in the unknown invisible momentum parameter space. In both of the plot yellow elliptical region is constrained area describing $q_{1z}(\vec{q}_{1T})$ and green elliptical region is constrained area for $q_{2z}(\vec{q}_{1T})$. Intersection region between these two constrained ellipse, shaded in white, is eligible for containing all the constraint $\hat{s}(\vec{q}_{1T})$ parameters as well as the true \hat{s} . Two other ends in this overlapping region would typically represent the \hat{s}_{min}^{cons} and \hat{s}_{max}^{cons} , with true \hat{s} in between them. Since \hat{s}_{min} does not have this additional constrain, it would be outside overlapping region and far from true \hat{s} . Inside the overlapping region \hat{s} contours are also presented where true CM energy is matches with the value of Higgs mass. The left figure shows one example event where \hat{s}^{True} is closer to \hat{s}_{min}^{cons} . This contributes at the endpoint of the \hat{s}_{min}^{cons} distribution and also giving better momentum reconstruction. The right figure shows another event where \hat{s}^{True} is close to the \hat{s}_{max}^{cons} contributing at the threshold of this distribution with better momentum reconstruction.

where M_{vi} is the invariant mass of visibles in the i -th decay chain, $i = 1, 2$. Missing transverse momentum constraints further permit us to rewrite them in terms of a single invisible particle transverse momentum components, which we choose as \vec{q}_{1T} for our examples. By simplifying the right hand side of the Eq. 5.1, one gets the equation of ellipse in terms of the transverse momenta and the parameters outside the ellipse are not physical with the given event. Two elliptical allowed regions for each event correspond to two side of decay chain and these two regions can not be completely disjoint from each other. All the available constraints in an event are satisfied only at the intersection region between them. Different situations can emerge for this overlapping region. Two ellipses may intersect each other over a finite region or a point (touching each other). In other case one ellipse may contain the other ellipse.

In Fig. 6 we consider such constrained regions demonstrated for two different events in antler topology. Each color shaded region is representing the allowed phase space by additional constrains in the unknown invisible momentum parameter space. Overlapping region between these two constrained ellipse is shaded in white where \hat{s} contours are also presented. One can identify the minimum value from this intersection region as \hat{s}_{min}^{cons} and the maximum value as \hat{s}_{max}^{cons} which reside at opposite ends within this region. Since \hat{s}^{True} also

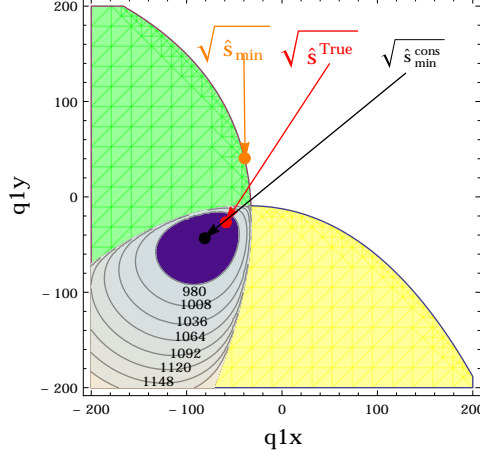


Figure 7: One example event demonstrating the invisible momentum reconstruction in case of non-antler topology through minimisation during construction of different \hat{s} variables. Description of shaded regions and mass variables are similar to previous figure.

satisfies all the constraints in the event it must also remain in the intersection region and in between these two constrained points⁵. Since the \hat{s}_{min} variable does not satisfy all additional constraints in the event, it would lie outside the intersection region and relatively far from true value. The left figure display one typical example event where \hat{s}^{True} is closer to \hat{s}_{min}^{cons} . This contributes at the endpoint of the \hat{s}_{min}^{cons} distribution and also giving better momentum reconstruction. The right figure shows another event where \hat{s}^{True} is close to the \hat{s}_{max}^{cons} contributing at the threshold of this distribution with better momentum reconstruction. In both figure, we depicted different colored dots for the the position (invisible momentums during minimisation or maximisation) of all \hat{s} variables together with actual \hat{s} correspond to that particular event. One can even read the corresponding values of these mass variables from their contours plotted within intersecting region. Similarly in Fig. 7 we have shown the momentum reconstruction capability of \hat{s}_{min}^{cons} and \hat{s}_{min} in an example of Non-Antler topology. The yellow and green shaded regions represents constrained $q_{1z}(\vec{q}_{1T})$ and $q_{2z}(\vec{q}_{1T})$ respectively and their intersection region is suitable for constrained \hat{s} . The red, orange and black point shows the true momenta and reconstructed momenta given by \hat{s}_{min} , \hat{s}_{min}^{cons} respectively.

We are now in a position to quantify the capability of momentum reconstruction. Fig. 8 exhibits the histogram showing the distributions for deviation of the reconstructed momentum from the corresponding true momentum as a fraction of true momentum $(q_i^{reconstructed} - q_i^{true})/|q_i^{true}|$ using both unconstrained and constrained \hat{s}_{min} methods. Left plot displays the momentum reconstruction capability in antler topology for transverse components of momentum. Similarly, right plot is for corresponding longitudinal component of the momentum. In each figure one histogram (in red bins) is shown for \hat{s}_{min} which agrees with corresponding analytical form. Also histograms with blue bins plotted in the same figure to display the momentum reconstruction capability using constrained minimisation \hat{s}_{min}^{cons} pointing out

⁵Eq. 5.1 reflects a four fold ambiguity from the longitudinal component in each event. However, the extremisation of constrained \hat{s} would qualify for a choice of unique momentum reconstruction.

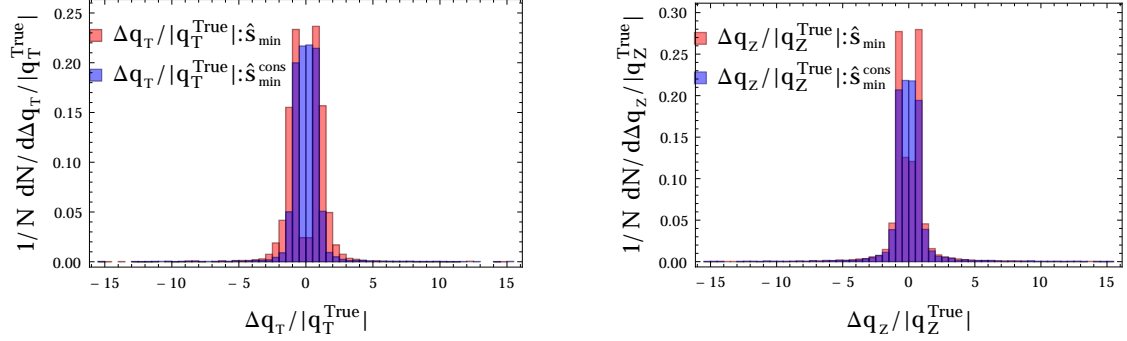


Figure 8: Histogram showing the distributions for deviation of the reconstructed momentum from the corresponding true momentum as a fraction of true momentum $(q_i^{reconstructed} - q_i^{true})/|q_i^{true}|$ using both unconstrained (red) and constrained (blue) \hat{s}_{min} methods. Left (right) plot displays the momentum reconstruction capability in antler topology for transverse (longitudinal) components of momentum. In each figure shown histograms one directly from \hat{s}_{min} for which agrees with corresponding analytical form, also shown histograms using constrained minimisation \hat{s}_{min}^{cons} to compare the improvements over unconstrained ones.

improvements over unconstrained ones.

We discussed the additional constraints in \hat{s}_{min} to choose the minimisation that gives reconstructed invisible momenta closer to their true values. To understand this consequence better, we look into the movements of these calculated momenta once we impose the constraints. In Fig. 9 we demonstrate through a correlation plot of constructed invisible momentum versus the corresponding true momentum taking few random representative event points. In both plots, each red dot point represents the calculated momentum derived from the \hat{s}_{min} against the corresponding true momentum for each event. Similarly, green dots are for corresponding momentum derived from the \hat{s}_{min}^{cons} . The purple arrows connecting from one red dot to other green dot represent the shift in the derived momentum once extra constraints are imposed. Since the true momentum is always same for a particular event, shifts due to minimisation in different mass variables are only horizontal. These arrows represent the degree of change due to constraints, shifting calculated momentums towards the diagonal true momentum points. Diagonal blue points the simply correlate true momenta with true momenta in each event to give the perspective how derived momenta composed against the true values. Left (right) plot corresponds to the transverse (longitudinal) momenta derived from \hat{s}_{min} and \hat{s}_{min}^{cons} .

6. Summary and conclusions

Large Hadron Collider started its extremely successful journey finding the long sought scalar.

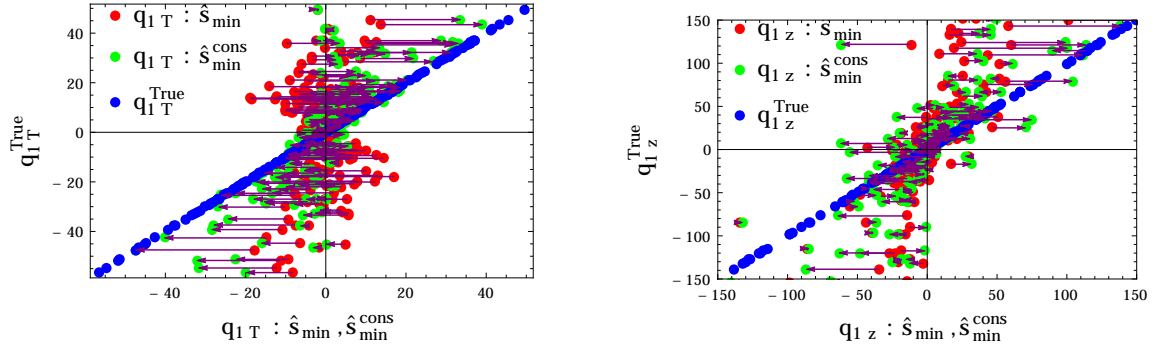


Figure 9: Correlation plot taking few random representative event points showing the shift of reconstructed transverse momenta (in left plot) and longitudinal momenta (in right plot) derived from \hat{s}_{\min} and $\hat{s}_{\min}^{\text{cons}}$. In both plots, each red dot point represents the calculated momentum derived from the \hat{s}_{\min} against the corresponding true momentum for each event. Similarly, green dots are for corresponding momentum derived from the $\hat{s}_{\min}^{\text{cons}}$. The purple arrows connecting from one red dot to other green dot represent the shift in the derived momentum once extra constraints are imposed. Diagonal blue points the simply correlate true momenta with true momenta in each event to give the perspective how derived momenta composed against the true values.

With no substantial evidence for BSM, expectation is high for next run of LHC. In the light of dark matter models, missing energy signals would be looked very carefully. The \hat{s}_{\min} variants of mass variables were designed for prompt finding of mass scale in a model independent way for any complex topology of BSM events associated with semi-invisible final production. In the present analysis, we proposed to exploit additional partial informations available in the event as constraints to improve the finding. We classified our discussions based on two different class of simple production topology widely available both in SM and BSM production, which are, antler and non-antler.

Different SM as well as new physics predicts antler production processes, including important Higgs production in the hadron collider. These topology can be constrained significantly using additional intermediate mass-shell conditions. We have demonstrated with different examples to show that the constrained variable $\hat{s}_{\min}^{\text{cons}}$ can significantly improve the distribution and the measurements. More interestingly, these additional constraints ensures a finite upper value of the \hat{s} variable, defined as, $\hat{s}_{\max}^{\text{cons}}$ which is not well-defined and finite in the unconstrained picture. Hence, this new variable also can be exploited up to some extend. Apart from considering different BSM example to demonstrate these variable in the context of sub-system topology and in the difficult signatures with more invisible final states in antler topology, we also demonstrated effect of these additional constraints in a simple non-antler topology.

To clarify the effects of these constraints in the invisible momenta parameter space, we choose phenomenological examples explicitly demonstrating how these mass variables are restricted and pushed towards the true values of \hat{s} , together with their choice the invisible momentums closer to that of true one. Hence, one can consider to quantify the capability of reconstructing the invisible momenta in present scenario. We constructed and shown the

efficiency of momentum reconstruction using these constrained \hat{s} variables which predicts a unique momenta associated with each of these mass-bound variables in each event. In conclusion, we explored the utility of additional informations we may already have, during exploration of the \hat{s} type mass variables which can be exploited with missing energy data at the LHC.

Acknowledgments

We would like to thank A. Datta for useful discussion during WHEPP XIII. P.K. also thanks RECAPP, HRI for hospitality where part of this work has been carried out.

References

- [1] Partha Konar, Kyoungchul Kong, and Konstantin T. Matchev. $\sqrt{\hat{s}_{min}}$: A Global inclusive variable for determining the mass scale of new physics in events with missing energy at hadron colliders. *JHEP*, 0903:085, 2009.
- [2] Partha Konar, Kyoungchul Kong, Konstantin T. Matchev, and Myeonghun Park. RECO level $\sqrt{\hat{s}_{min}}$ and subsystem $\sqrt{\hat{s}_{min}}$: Improved global inclusive variables for measuring the new physics mass scale in \cancel{E}_T events at hadron colliders. *JHEP*, 1106:041, 2011.
- [3] Serguei Chatrchyan et al. Observation of a new boson at a mass of 125 GeV with the CMS experiment at the LHC. *Phys.Lett.*, B716:30–61, 2012.
- [4] Georges Aad et al. Observation of a new particle in the search for the Standard Model Higgs boson with the ATLAS detector at the LHC. *Phys.Lett.*, B716:1–29, 2012.
- [5] G. Hinshaw et al. Nine-Year Wilkinson Microwave Anisotropy Probe (WMAP) Observations: Cosmological Parameter Results. *Astrophys.J.Suppl.*, 208:19, 2013.
- [6] Alan J. Barr and Christopher G. Lester. A Review of the Mass Measurement Techniques proposed for the Large Hadron Collider. *J.Phys.*, G37:123001, 2010.
- [7] A.J. Barr, T.J. Khoo, P. Konar, K. Kong, C.G. Lester, et al. Guide to transverse projections and mass-constraining variables. *Phys.Rev.*, D84:095031, 2011.
- [8] Kyoungchul Kong. Measuring Properties of Dark Matter at the LHC. *AIP Conf.Proc.*, 1604:381–388, 2014.
- [9] Won Sang Cho, Doojin Kim, Konstantin T. Matchev, and Myeonghun Park. Probing Resonance Decays to Two Visible and Multiple Invisible Particles. *Phys.Rev.Lett.*, 112(21):211801, 2014.
- [10] Kaustubh Agashe, Doojin Kim, Manuel Toharia, and Devin G.E. Walker. Distinguishing Dark Matter Stabilization Symmetries Using Multiple Kinematic Edges and Cusps. *Phys.Rev.*, D82:015007, 2010.
- [11] Kaustubh Agashe, Doojin Kim, Devin G.E. Walker, and Lijun Zhu. Using M_{T2} to Distinguish Dark Matter Stabilization Symmetries. *Phys.Rev.*, D84:055020, 2011.
- [12] Gian Francesco Giudice, Ben Gripaios, and Rakhi Mahbubani. Counting dark matter particles in LHC events. *Phys.Rev.*, D85:075019, 2012.

- [13] Yang Bai and Hsin-Chia Cheng. Identifying Dark Matter Event Topologies at the LHC. *JHEP*, 1106:021, 2011.
- [14] Monika Blanke, David Curtin, and Maxim Perelstein. SUSY-Yukawa Sum Rule at the LHC. *Phys.Rev.*, D82:035020, 2010.
- [15] Arvind Rajaraman and Felix Yu. A New Method for Resolving Combinatorial Ambiguities at Hadron Colliders. *Phys.Lett.*, B700:126–132, 2011.
- [16] Philip Baringer, Kyoungchul Kong, Mathew McCaskey, and Daniel Noonan. Revisiting Combinatorial Ambiguities at Hadron Colliders with M_{T2} . *JHEP*, 1110:101, 2011.
- [17] Kiwoon Choi, Diego Guadagnoli, and Chan Beom Park. Reducing combinatorial uncertainties: A new technique based on MT2 variables. *JHEP*, 1111:117, 2011.
- [18] G.L. Bayatian et al. CMS technical design report, volume II: Physics performance. *J.Phys.*, G34:995–1579, 2007.
- [19] I. Hinchliffe, F.E. Paige, M.D. Shapiro, J. Soderqvist, and W. Yao. Precision SUSY measurements at CERN LHC. *Phys.Rev.*, D55:5520–5540, 1997.
- [20] B.K. Gjelsten, D.J. Miller, and P. Osland. Measurement of SUSY masses via cascade decays for SPS 1a. *JHEP*, 0412:003, 2004.
- [21] B.C. Allanach, C.G. Lester, Michael Andrew Parker, and B.R. Webber. Measuring sparticle masses in nonuniversal string inspired models at the LHC. *JHEP*, 0009:004, 2000.
- [22] Mihoko M. Nojiri, Daisuke Toya, and Tomio Kobayashi. Lepton energy asymmetry and precision SUSY study at hadron colliders. *Phys.Rev.*, D62:075009, 2000.
- [23] B.K. Gjelsten, D.J. Miller, and P. Osland. Measurement of the gluino mass via cascade decays for SPS 1a. *JHEP*, 0506:015, 2005.
- [24] Michael Burns, Konstantin T. Matchev, and Myeonghun Park. Using kinematic boundary lines for particle mass measurements and disambiguation in SUSY-like events with missing energy. *JHEP*, 0905:094, 2009.
- [25] Konstantin T. Matchev, Filip Moortgat, Luc Pape, and Myeonghun Park. Precise reconstruction of sparticle masses without ambiguities. *JHEP*, 0908:104, 2009.
- [26] M.M. Nojiri, G. Polesello, and D.R. Tovey. Proposal for a new reconstruction technique for SUSY processes at the LHC. 2003.
- [27] K. Kawagoe, M.M. Nojiri, and G. Polesello. A New SUSY mass reconstruction method at the CERN LHC. *Phys.Rev.*, D71:035008, 2005.
- [28] Hsin-Chia Cheng, John F. Gunion, Zhenyu Han, Guido Marandella, and Bob McElrath. Mass determination in SUSY-like events with missing energy. *JHEP*, 0712:076, 2007.
- [29] Mihoko M. Nojiri and Michihisa Takeuchi. Study of the top reconstruction in top-partner events at the LHC. *JHEP*, 0810:025, 2008.
- [30] Hsin-Chia Cheng, Dalit Engelhardt, John F. Gunion, Zhenyu Han, and Bob McElrath. Accurate Mass Determinations in Decay Chains with Missing Energy. *Phys.Rev.Lett.*, 100:252001, 2008.
- [31] Lars Sonnenschein. Analytical solution of $t\bar{t}$ dilepton equations. *Phys.Rev.*, D73:054015, 2006.

- [32] C.G. Lester and D.J. Summers. Measuring masses of semiinvisibly decaying particles pair produced at hadron colliders. *Phys.Lett.*, B463:99–103, 1999.
- [33] Alan Barr, Christopher Lester, and P. Stephens. $m(T2)$: The Truth behind the glamour. *J.Phys.*, G29:2343–2363, 2003.
- [34] Patrick Meade and Matthew Reece. Top partners at the LHC: Spin and mass measurement. *Phys.Rev.*, D74:015010, 2006.
- [35] Christopher Lester and Alan Barr. MTGEN: Mass scale measurements in pair-production at colliders. *JHEP*, 0712:102, 2007.
- [36] Won Sang Cho, Kiwoon Choi, Yeong Gyun Kim, and Chan Beom Park. Gluino Stransverse Mass. *Phys.Rev.Lett.*, 100:171801, 2008.
- [37] Won Sang Cho, Kiwoon Choi, Yeong Gyun Kim, and Chan Beom Park. Measuring superparticle masses at hadron collider using the transverse mass kink. *JHEP*, 0802:035, 2008.
- [38] Alan J. Barr, Ben Gripaios, and Christopher G. Lester. Weighing Wimps with Kinks at Colliders: Invisible Particle Mass Measurements from Endpoints. *JHEP*, 0802:014, 2008.
- [39] Ben Gripaios. Transverse observables and mass determination at hadron colliders. *JHEP*, 0802:053, 2008.
- [40] Mihoko M. Nojiri, Yasuhiro Shimizu, Shogo Okada, and Kiyotomo Kawagoe. Inclusive transverse mass analysis for squark and gluino mass determination. *JHEP*, 0806:035, 2008.
- [41] Michael Burns, Kyoungchul Kong, Konstantin T. Matchev, and Myeonghun Park. Using Subsystem MT2 for Complete Mass Determinations in Decay Chains with Missing Energy at Hadron Colliders. *JHEP*, 0903:143, 2009.
- [42] Won Sang Cho, Jihn E. Kim, and Ji-Hun Kim. Amplification of endpoint structure for new particle mass measurement at the LHC. *Phys.Rev.*, D81:095010, 2010.
- [43] Won Sang Cho, William Klemm, and Mihoko M. Nojiri. Mass measurement in boosted decay systems at hadron colliders. *Phys.Rev.*, D84:035018, 2011.
- [44] Partha Konar, Kyoungchul Kong, Konstantin T. Matchev, and Myeonghun Park. Superpartner Mass Measurement Technique using 1D Orthogonal Decompositions of the Cambridge Transverse Mass Variable M_{T2} . *Phys.Rev.Lett.*, 105:051802, 2010.
- [45] Alan J. Barr, Ben Gripaios, and Christopher G. Lester. Transverse masses and kinematic constraints: from the boundary to the crease. *JHEP*, 0911:096, 2009.
- [46] Partha Konar, Kyoungchul Kong, Konstantin T. Matchev, and Myeonghun Park. Dark Matter Particle Spectroscopy at the LHC: Generalizing $M(T2)$ to Asymmetric Event Topologies. *JHEP*, 1004:086, 2010.
- [47] Colin H. Lally and Christopher G. Lester. Properties of $MT2$ in the massless limit. 2012.
- [48] Daniel R. Tovey. On measuring the masses of pair-produced semi-invisibly decaying particles at hadron colliders. *JHEP*, 0804:034, 2008.
- [49] Giacomo Polesello and Daniel R. Tovey. Supersymmetric particle mass measurement with the boost-corrected contranverse mass. *JHEP*, 1003:030, 2010.
- [50] Mario Serna. A Short comparison between $m(T2)$ and $m(CT)$. *JHEP*, 0806:004, 2008.

- [51] Konstantin T. Matchev and Myeonghun Park. A General method for determining the masses of semi-invisibly decaying particles at hadron colliders. *Phys.Rev.Lett.*, 107:061801, 2011.
- [52] Rakhi Mahbubani, Konstantin T. Matchev, and Myeonghun Park. Re-interpreting the Oxbridge stransverse mass variable MT2 in general cases. *JHEP*, 1303:134, 2013.
- [53] Won Sang Cho, James S. Gainer, Doojin Kim, Konstantin T. Matchev, Filip Moortgat, et al. On-shell constrained M_2 variables with applications to mass measurements and topology disambiguation. *JHEP*, 1408:070, 2014.
- [54] D.R. Tovey. Measuring the SUSY mass scale at the LHC. *Phys.Lett.*, B498:1–10, 2001.
- [55] Jay Hubisz, Joseph Lykken, Maurizio Pierini, and Maria Spiropulu. Missing energy look-alikes with 100 pb⁻¹ at the LHC. *Phys.Rev.*, D78:075008, 2008.
- [56] Won Sang Cho, Kiwoon Choi, Yeong Gyun Kim, and Chan Beom Park. M(T2)-assisted on-shell reconstruction of missing momenta and its application to spin measurement at the LHC. *Phys.Rev.*, D79:031701, 2009.
- [57] Chan Beom Park. Reconstructing the heavy resonance at hadron colliders. *Phys.Rev.*, D84:096001, 2011.
- [58] Andreas Papaefstathiou and Bryan Webber. Effects of QCD radiation on inclusive variables for determining the scale of new physics at hadron colliders. *JHEP*, 0906:069, 2009.
- [59] Andreas Papaefstathiou and Bryan Webber. Effects of invisible particle emission on global inclusive variables at hadron colliders. *JHEP*, 1007:018, 2010.
- [60] A. Barr, T. Khoo, P. Konar, K. Kong, C. Lester, et al. A Storm in a 'T' Cup. *AIP Conf.Proc.*, 1441:722–724, 2012.
- [61] Abdelhak Djouadi. The Anatomy of electro-weak symmetry breaking. II. The Higgs bosons in the minimal supersymmetric model. *Phys.Rept.*, 459:1–241, 2008.
- [62] Mirjam Cvetič and P. Langacker. Z-prime physics and supersymmetry. *Adv.Ser.Direct.High Energy Phys.*, 21:325–350, 2010.
- [63] Matthew Baumgart, Thomas Hartman, Can Kilic, and Lian-Tao Wang. Discovery and measurement of sleptons, binos, and winos with a Z-prime. *JHEP*, 0711:084, 2007.
- [64] Asesh Krishna Datta, Kyoungchul Kong, and Konstantin T. Matchev. Discrimination of supersymmetry and universal extra dimensions at hadron colliders. *Phys.Rev.*, D72:096006, 2005.
- [65] Hsin-Chia Cheng, Jonathan L. Feng, and Konstantin T. Matchev. Kaluza-Klein dark matter. *Phys.Rev.Lett.*, 89:211301, 2002.
- [66] Gulab Bambhaniya, Joydeep Chakraborty, Srubabati Goswami, and Partha Konar. Generation of neutrino mass from new physics at TeV scale and multilepton signatures at the LHC. *Phys.Rev.*, D88(7):075006, 2013.
- [67] Tao Han, Ian-Woo Kim, and Jeonghyeon Song. Kinematic Cusps: Determining the Missing Particle Mass at Colliders. *Phys.Lett.*, B693:575–579, 2010.
- [68] Tao Han, Ian-Woo Kim, and Jeonghyeon Song. Kinematic Cusps With Two Missing Particles I: Antler Decay Topology. *Phys.Rev.*, D87(3):035003, 2013.

- [69] Tao Han, Ian-Woo Kim, and Jeonghyeon Song. Kinematic Cusps with Two Missing Particles II: Cascade Decay Topology. *Phys.Rev.*, D87(3):035004, 2013.
- [70] Neil D. Christensen, Tao Han, Zhuoni Qian, Josh Sayre, Jeonghyeon Song, et al. Determining the Dark Matter Particle Mass through Antler Topology Processes at Lepton Colliders. *Phys.Rev.*, D90:114029, 2014.